

Phonons in GaAs/AlAs superlattices grown along the [111] direction

Z. V. Popović* and M. Cardona

Max-Planck-Institut für Festkörperforschung, Postfach 80 06 65, D-7000 Stuttgart 80, Federal Republic of Germany

E. Richter and D. Strauch

Institut für Theoretische Physik, Universität Regensburg, D-8400 Regensburg, Federal Republic of Germany

L. Tapfer and K. Ploog

Max-Planck-Institut für Festkörperforschung, Postfach 80 06 65, D-7000 Stuttgart 80, Federal Republic of Germany

(Received 11 October 1989)

We present Raman-scattering data for GaAs/AlAs superlattices grown on GaAs substrates along the [111] direction. The appearance of distinct x-ray satellite peaks around the Bragg reflections demonstrates the formation of highly ordered periodic superlattice structures. The confined optical-phonon modes have frequencies which map closely those of the parent materials in the [111] direction of \mathbf{k} space. We also observe folded acoustic-phonon modes. The results of a lattice-dynamical calculation for these superlattices on the basis of the shell model are presented, with special emphasis on the angular dispersion of "interface" modes.

I. INTRODUCTION

The optical properties of GaAs/AlAs superlattices have been of great interest in the last ten years. Most studies reported so far have been performed on material grown on [001]-oriented GaAs substrates. However, recently it has been reported that device-quality GaAs/AlAs superlattices can be grown by molecular-beam epitaxy (MBE) on any low-index crystallographic plane: (110),^{1,2} (012),³⁻⁵ (111),⁶⁻⁹ and (211).¹⁰ Besides this, it has been shown⁶ that GaAs/Al_xGa_{1-x}As quantum-well (QW) structures grown along the [111] direction have better optical properties than [001] GaAs/AlAs quantum-well heterostructures (the photoluminescence intensity of the [111] GaAs/Al_xGa_{1-x}As single QW is about 50 times higher than that of a [001] single QW). The enhancement of quantum effects in [111] GaAs/Al_xGa_{1-x}As QW structures may find important applications in optoelectronics as it opens the possibility of making QW lasers with greater emission efficiency.^{7,8}

The vibrational properties of GaAs/AlAs superlattices grown along the [001] direction are well known (for a review, see Ref. 11, where references to further work can be found), and those of GaAs/AlAs superlattices grown along the [110] (Ref. 1) and [012] (Refs. 3-5) directions were considered by us in recent papers. In this paper we present the results of x-ray- and Raman-scattering investigations of a GaAs/AlAs superlattice grown along the [111] direction together with a theoretical discussion of its lattice dynamics.

This paper is organized as follows. After a brief description of the growth procedure and x-ray characterization (Sec. II), we consider symmetry and selection rules for Raman scattering by the [111] GaAs/AlAs superlattices (Sec. III). Experimental results are presented and discussed in Sec. IV. In Sec. V the lattice dynamics of the [111] GaAs/AlAs superlattice, calculated using the shell model, is reported with special emphasis on the an-

gular dispersion of the interface modes. Section VI contains the summary.

II. EXPERIMENT

The sample studied here was grown by molecular-beam epitaxy (MBE) on a 0.5° misoriented (111)*B* GaAs (arsenic-terminated surface) substrate kept at a temperature of 530°C, which was mounted side by side with a (001)-oriented reference substrate. The growth rates of 0.5 monolayer/s for GaAs and 0.4 monolayer/s for AlAs were determined precisely for the growth on the (001) substrate from the period of the intensity oscillations of the specular beam in the reflection high-energy electron-diffraction (RHEED) pattern. To improve the formation of abrupt interfaces, the growth was stopped for 10 s when changing from GaAs to AlAs, and vice versa. The sample grown in this way consists of 100 periods of alternating GaAs and AlAs layers deposited on a 0.25- μm buffer layer.

The x-ray-diffraction pattern of the [111] GaAs/AlAs superlattice was recorded by using a single-crystal goniometer operating in θ - 2θ coupling and with a post-sample curved graphite monochromator. The diffraction patterns were recorded in the vicinity of the (111), (222), and (333) GaAs reflections using Cu $K\alpha$ radiation.

The diffraction patterns in the vicinity of the (111) reflection point, Fig. 1(a), exhibit strong first-order satellite peaks. First-order satellites are also observed at the (222) reflection, Fig. 1(b). The angular distance between these satellites is a measure of the superlattice (SL) period length λ_{SL} .¹² The intensity of each satellite peak is related to the structure factor F_{SL} of one superlattice unit cell by the equation¹²

$$F_{\text{SL}}(H) = 2 \left[(f_{\text{Ga}} + f_{\text{As}} R_1^{1/4}) \frac{R_1^{n_1} - 1}{R_1 - 1} + (f_{\text{Al}} + f_{\text{As}} R_2^{1/4}) \frac{R_1^{n_1} (R_2^{n_2} - 1)}{R_2 - 1} \right]$$

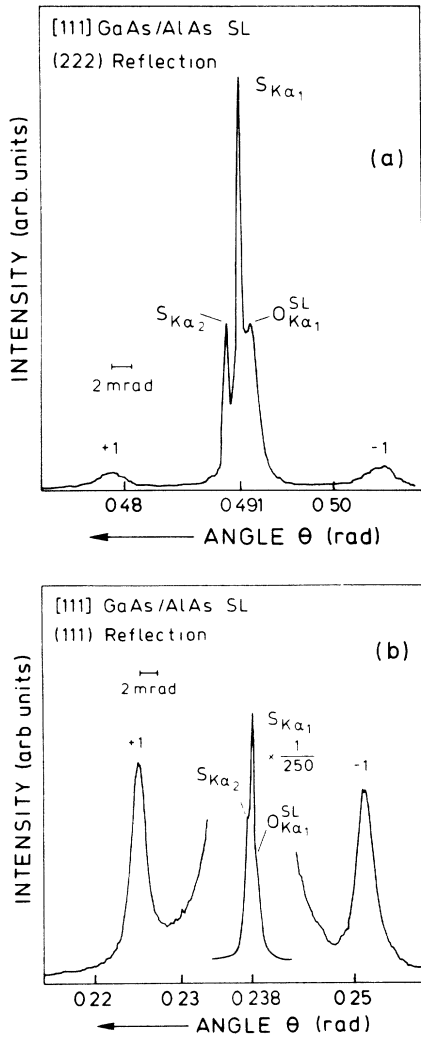


FIG. 1. Single-crystal x-ray-diffraction pattern of the [111] $(\text{GaAs})_9/(\text{AlAs})_{10}$ superlattice recorded in the vicinity of (a) the (111) and (b) (222) GaAs reciprocal-lattice points. S denotes the substrate, O the superlattice main reflection, and ± 1 the superlattice satellites.

with $R_j = \exp(i4\pi H_{\parallel} d_j / \lambda_{\text{SL}})$, where H_{\parallel} is the component in the SL growth direction of the reciprocal-lattice point $\mathbf{H} = (h, k, l)$, f_{Ga} , f_{Al} , and f_{As} are the atomic-scattering factors of the Ga, Al, and As atoms, respectively, while d_1 (d_2) and n_1 (n_2) are the thickness and number of GaAs (AlAs) monolayers, respectively, in the SL unit cell.

By fitting the experimental intensity ratio of the $+1$ and -1 satellites in Fig. 1(a) with the equation given above, we determined the number of GaAs and AlAs monolayers in one SL unit cell. For the present case we found that the superlattice is composed of nine GaAs and ten AlAs monolayers; each monolayer of the [111] GaAs/AlAs superlattice is $d_1 = d_2 = a_0 \sqrt{3}/3 \approx 3.26$ Å thick, the actual superlattice period length λ_{SL} being the sum of $n_1 d_1 = 29.4$ Å (GaAs) and $n_2 d_2 = 32.6$ Å (AlAs). The same results were obtained by evaluating the (222) direction pattern, Fig. 1(b).

The Raman spectra were measured in the backscatter-

ing geometry using a Spex Industries double monochromator (model 1404) with a conventional photon-counting system. The excitation-light sources were the 5145- and 4579-Å lines of an Ar^+ -ion laser. Measurements were made at both 300 and 15 K.

III. SYMMETRY AND SELECTION RULES

In earlier papers^{1,3-5,11} it has been demonstrated that superperiodicity in the [001], [110], or [012] direction induces a lowering of the crystal symmetry from cubic to tetragonal (point group D_{2d}), orthorhombic (point group C_{2v}), or monoclinic (point group C_2), respectively. For the superperiodicity in the [111] direction the symmetry is trigonal (point group C_{3v}). Depending on the number of GaAs (n_1) or AlAs (n_2) monolayers, the [111] $(\text{GaAs})_{n_1}/(\text{AlAs})_{n_2}$ superlattices appear in two different space groups,

$$C_{3v}^1 (P3m) \text{ for } (n_1 + n_2)/3 = k,$$

$$C_{3v}^5 (R3m) \text{ for } (n_1 + n_2)/3 \neq k,$$

where k is any integer. Note that the primitive cell of the former is trigonal, that of the latter rhombohedral.

Schematic projections of the Ga(Al)As layers on the (111) and $(\bar{1}\bar{1}0)$ planes are displayed in Figs. 2(a) and 2(b) together with the symmetry elements of the C_{3v} point group: the threefold axes (C_3) are parallel to a [111] axis of the constituents while the mirror planes are parallel to the (011), $(0\bar{1}1)$, and $(\bar{1}\bar{1}0)$ planes, respectively; see Fig. 2(a).

In the zinc-blende structure the phonons with wave vectors \mathbf{q} in the [111] direction have pure longitudinal (z' , parallel to [111]) and pure transverse (x' , parallel to $[\bar{1}\bar{1}0]$, or y' , parallel to $[11\bar{2}]$) polarizations. For $\mathbf{q} \parallel [001]$ the transverse modes are degenerate. The same is true for these modes in [111] superlattices for $\mathbf{q} \parallel [111]$. This property does not hold for [110] and [012] superlattices.

With respect to the C_{3v} point group the longitudinal and transverse modes have A_1 and E symmetry, respectively. The Raman tensors for the optical modes, as carried over from those of the bulk crystals (at bulk wave vector $\mathbf{k} = 0$), are in the (x, y, z) coordinate system

$$\underline{R}(LO) = \frac{1}{\sqrt{3}} \begin{pmatrix} 0 & d & d \\ d & 0 & d \\ d & d & 0 \end{pmatrix},$$

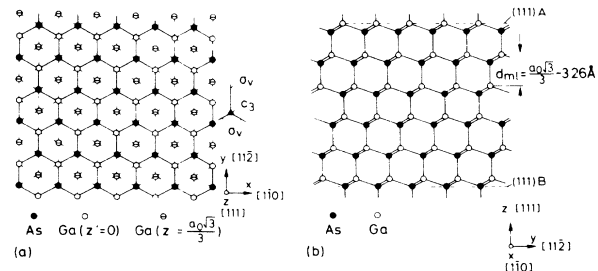


FIG. 2. (111) GaAs (AlAs) layers viewed along the (a) [111] and (b) $[\bar{1}\bar{1}0]$ directions. The symmetry elements of the C_{3v} point group ($C_3, 3\sigma_v$) are also indicated.

$$\underline{R}(TO_{x'}) = \frac{1}{\sqrt{2}} \begin{pmatrix} 0 & 0 & -d \\ 0 & 0 & d \\ -d & d & 0 \end{pmatrix}, \quad (1)$$

$$\underline{R}(TO_{y'}) = \frac{1}{\sqrt{6}} \begin{pmatrix} 0 & -2d & d \\ -2d & 0 & d \\ d & d & 0 \end{pmatrix}.$$

Besides the Raman tensors given by Eq. (1), we must also include the tensor

$$\underline{R}_F = \begin{pmatrix} a & 0 & 0 \\ 0 & a & 0 \\ 0 & 0 & a \end{pmatrix}, \quad (2)$$

which results from the Fröhlich interaction for LO phonons.

The corresponding Raman-polarization rules for backscattering off the (111) surface of the parent material are given in Table I. The same selection rules can be applied to the [111] GaAs/AlAs superlattices, with no additional symmetry conditions of confinement of the superlattice modes. Namely, similar to the other GaAs/AlAs superlattices one can assign effective wave vectors

$$q_m = \frac{m}{n_i + \gamma} \frac{\pi\sqrt{3}}{a_0} \quad (3)$$

to modes confined to the constituents. In Eq. (3) n_i is the number of GaAs or AlAs monolayers, respectively, and γ describes the extent to which the modes confined to one (GaAs) layer penetrate into the other (AlAs). We have found $\gamma \simeq 0.5$ in the present case; see below. In the backscattering configuration with polarizations along both the $[1\bar{1}0]$ or $[11\bar{2}]$ directions the A_1 and E modes are allowed (see Table I) regardless of whether m is even and odd. For the depolarized configuration only the E modes are allowed again with m either even or odd [note the contrast to the [001] and [012] superlattices for which the mechanisms of Eqs. (1) and (2) are allowed only for m odd or even, respectively].

In order to determine the Raman selection rules for the folded acoustic phonons of the [111] superlattices, we start from the Brillouin tensors of the bulk crystals. For $\mathbf{q} \parallel [111]$ the long-wavelength acoustic waves have purely longitudinal and transverse character, and the two transverse modes are degenerate.

The corresponding Brillouin tensors for the TA and LA components for $\mathbf{q} \parallel [111]$ are

$$\underline{R}(LA) = \frac{\epsilon_0^2}{3} \begin{pmatrix} p_{\parallel} & 2p_{44} & 2p_{44} \\ 2p_{44} & p_{\parallel} & 2p_{44} \\ 2p_{44} & 2p_{44} & p_{\parallel} \end{pmatrix},$$

$$\underline{R}(TA_{x'}) = \frac{\epsilon_0^2}{\sqrt{6}} \begin{pmatrix} p_{\perp} & 0 & p_{44} \\ 0 & -p_{\perp} & -p_{44} \\ p_{44} & -p_{44} & 0 \end{pmatrix}, \quad (4)$$

$$\underline{R}(TA_{y'}) = \frac{\epsilon_0^2}{3\sqrt{2}} \begin{pmatrix} p_{\perp} & 2p_{44} & -p_{44} \\ 2p_{44} & p_{\perp} & -p_{44} \\ -p_{44} & -p_{44} & -2p_{\perp} \end{pmatrix},$$

with

$$p_{\parallel} = p_{11} + 2p_{12},$$

$$p_{\perp} = p_{11} - p_{12},$$

where p_{ij} are the elasto-optic coefficients and ϵ_0 is the dielectric constant. The corresponding selection rules for acoustic folded phonons are also given in Table I. For the [111] GaAs/AlAs superlattices both longitudinal and transverse folded acoustic phonons are Raman active in backscattering.

IV. RAMAN-SCATTERING SPECTRA

A. Confined phonons

Figure 3 shows the Raman spectra of the [111] (GaAs)₉/(AlAs)₁₀ sample for all three polarizations obtained at 15 K with the 5145-Å line, away from all resonances. For backscattering with both polarizations along the x' or y' directions, we obtain the type of spectra expected from the selection rules of Table I. The peaks labeled LO_m correspond to the confined longitudinal-optical modes localized in the GaAs and AlAs slabs. Besides the LO_m confined phonons, TO_m confined modes are also clearly observed in Fig. 3. For the depolarized configuration only transverse modes are Raman active. In the GaAs optical-phonon region the confined TO_m modes (labeled tentatively with $m=1,2$, and 3) are observed, while in the AlAs optical region only the TO_1

TABLE I. Polarization selection rules in backscattering geometry for optical and acoustical phonons of GaAs/AlAs superlattices grown along the [111] direction as carried over from those for the bulk materials; a represents interband Fröhlich, d the deformation potential terms, $e = (p_{11} - p_{12} - 2p_{44})\epsilon_0^2/3\sqrt{2}$, and $f = (p_{11} + 2p_{12} - 2p_{44})\epsilon_0^2/3$, where p_{ij} are elasto-optic constants.

| Configuration | Polarization | | Light-scattering cross-section | | | | |
|--------------------|---------------|---------------|--------------------------------|---------------------------|------------------|-----------|-------|
| | Incident | Scattering | Optical phonons | | Acoustic phonons | | |
| | | | A_1 | E | $TA_{x'}$ | $TA_{y'}$ | LA |
| $z'(x'x')\bar{z}'$ | $[1\bar{1}0]$ | $[1\bar{1}0]$ | $a^2 + \frac{1}{3}d^2(LO)$ | $\frac{2}{3}d^2(TO_{y'})$ | 0 | e^2 | f^2 |
| $z'(x'y')\bar{z}'$ | $[1\bar{1}0]$ | $[11\bar{2}]$ | | $\frac{2}{3}d^2(TO_{x'})$ | e^2 | 0 | 0 |
| $z'(y'y')\bar{z}'$ | $[11\bar{2}]$ | $[11\bar{2}]$ | $a^2 + \frac{1}{3}d^2(LO)$ | $\frac{2}{3}d^2(TO_{y'})$ | 0 | e^2 | f^2 |

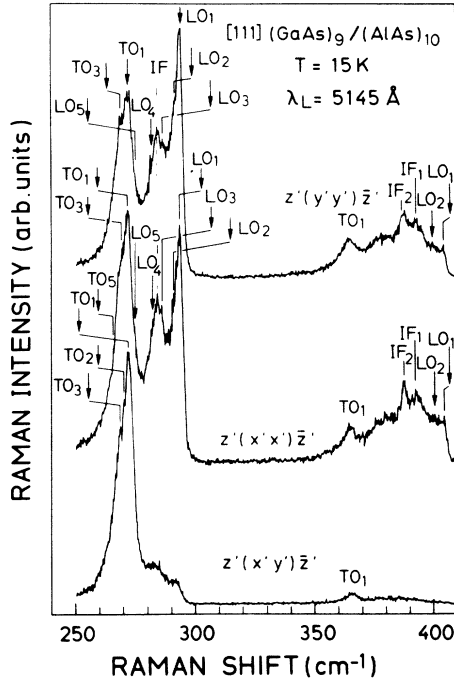


FIG. 3. Raman spectra of a [111] (GaAs)₉/(AlAs)₁₀ superlattice at 15 K in different backscattering configurations ($\mathbf{x}'\parallel[1\bar{1}0]$, $\mathbf{y}'\parallel[11\bar{2}]$, $\mathbf{z}'\parallel[111]$). The exciting-laser frequency (5145 Å) is away from all resonances.

confined mode is seen. Besides LO_m and TO_m confined phonons, one additional mode in the GaAs and two additional ones in the AlAs optical-phonon region (labeled IF, IF₁, and IF₂) are attributed to interface modes (see below).¹³

Using the assignment of observed Raman peaks to confined LO and TO modes, we compare the corresponding frequencies with the dispersion relations of bulk GaAs and AlAs calculated along the Γ - L direction using the shell model C(ii) of Dolling and Waugh¹⁴ with parameters which give the best fit to recent low-temperature high-precision neutron data for GaAs.¹⁵ The corresponding dispersion relations for AlAs were described by the same model with only the mass of the cation being changed. Figures 4(a) and 4(b) show the calculated dispersion curves of bulk GaAs and AlAs together with the measured frequencies of LO_m and TO_m phonons versus q_m [obtained from Eq. (3) with $\gamma=0.5$]. In the same figure, the plotted bars represent the magnitude of the “optical-like” weighted displacements¹⁶

$$m_a \mathbf{u}_a(\mathbf{q}j) - m_c \mathbf{u}_c(\mathbf{q}j) \quad (5)$$

in terms of their components along the three directions [111], $[1\bar{1}0]$, and $[11\bar{2}]$, where \mathbf{u}_k and m_k are the displacements and masses of the anion ($k=a$) and cation ($k=c$), respectively. This representation illustrates the pure polarization character of LO and TO vibrational modes.

For GaAs-like optical phonons, as seen from Fig. 4(a), the agreement between our experimental data and the theoretical predictions is excellent, a fact which confirms the m assignment given above. In the AlAs optical region the difference between experimental and theoretical

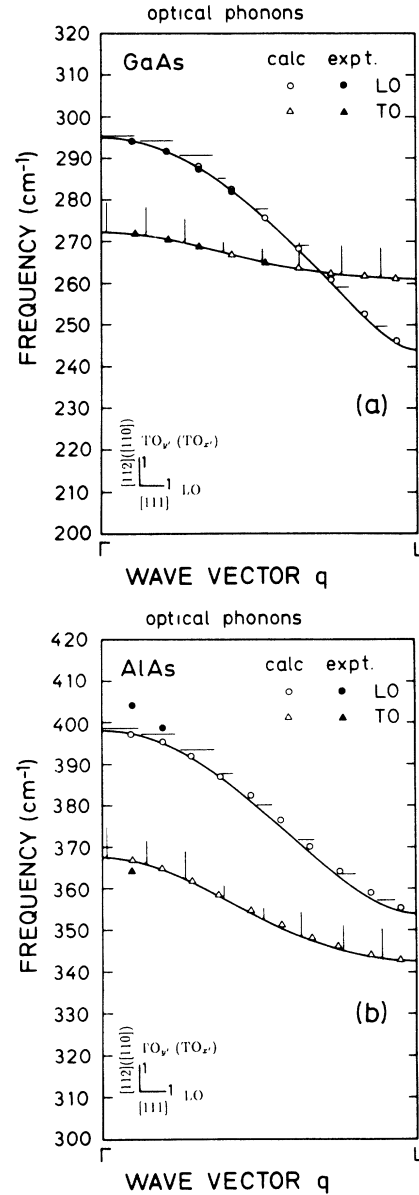


FIG. 4. Experimental (\bullet, \blacktriangle) and calculated (\circ, \triangle) confined-mode frequencies as a function of confinement wave vector q_m , Eq. (3), together with theoretical optical-phonon dispersion curves of (a) bulk GaAs and (b) AlAs in the Γ - L direction and the projections of the corresponding phonon displacement of the cation relative to the nearest anion [Eq. (5)] along the [111] and $[1\bar{1}0]$ (or $[11\bar{2}]$) directions. q is in units of $\pi\sqrt{3}/a_0$.

frequencies is about 6 cm^{-1} (typical also for [001], [110], and [012] GaAs/AlAs superlattices^{1,4,11}). We believe that this difference originates from insufficient accuracy of the calculated dispersion curves of bulk AlAs, for which no neutron data are available.

B. Folded acoustic phonons

The velocities of the longitudinal and transverse bulk sound waves for $\mathbf{q}\parallel[111]$ are¹⁷

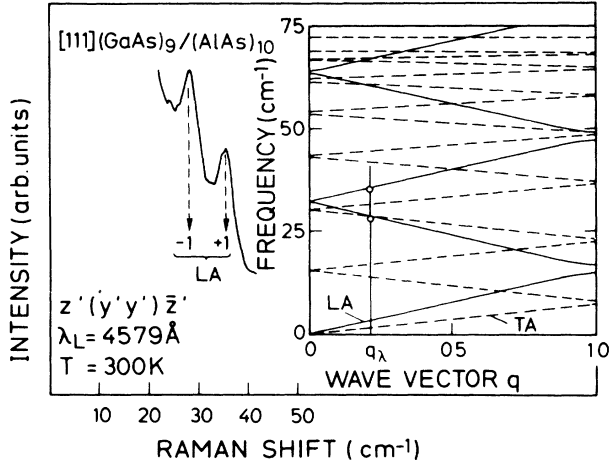


FIG. 5. Raman spectra of a [111] $(\text{GaAs})_9/(\text{AlAs})_{10}$ superlattice in the region from 20 to 45 cm^{-1} measured with the 4579-Å line of an Ar^+ -ion laser at 300 K. The inset shows shell-model results for folded-phonon dispersion curves together with the experimentally observed (\circ) folded-LA-phonon frequencies. q is in units of $\pi\sqrt{3}/a_0$.

$$v_{\text{long}} = [(C_{11} + 2C_{12} + 4C_{44})/3\rho]^{1/2},$$

$$v_{\text{trans}} = [(C_{11} - 2C_{12} + C_{44})/3\rho]^{1/2},$$

where C_{11} , C_{12} , and C_{44} are the stiffness constants and ρ the mass density.

As predicted by the selection rules of Table I, folded acoustic modes with both longitudinal and transverse polarizations are Raman active in backscattering for [111]-oriented GaAs/AlAs superlattices. Figure 5 shows the Raman spectra for $z'(x'x')z'$ polarization in the spectral range between 20 and 45 cm^{-1} obtained at 300 K with the 4579-Å line of an Ar^+ laser. The doublet $(-1, +1)$ of folded LA-phonon modes at 28.7 and 35.5 cm^{-1} is clearly observed. According to shell-model calculations (inset of Fig. 5) a folded-TA-phonon doublet should be located at about 15 cm^{-1} . Unfortunately, these phonons were not observed, possibly because they are masked by elastically scattered light.

We compare in Fig. 5 the frequency of the observed folded-phonon modes with a calculation based on the shell model. Folded-phonon dispersion curves calculated with this model are given in the inset of Fig. 5 together with the experimental frequencies obtained with the 4579-Å line of an Ar^+ -ion laser. As can be seen from this figure, our experimental data for folded LA phonons with $q \parallel [111]$ are fully in agreement with the shell-model calculation, which is a consequence of the fact that the shell model reproduces the appropriate stiffness constant¹⁸ correctly. It is interesting to note that the $(-1, +1)$ splitting of LA doublets is 5, 6.5, and 7 cm^{-1} for [001]-, [110]-, and [111]-oriented GaAs/AlAs superlattices, respectively, in accordance with the dependence of the sound velocities on the propagation direction in the bulk materials.¹⁸

V. LATTICE DYNAMICS OF THE [111] GaAs/AlAs SUPERLATTICE

Lattice-dynamical calculations were performed for the [111] $(\text{GaAs})_9/(\text{AlAs})_{10}$ superlattice using the shell model¹⁴ previously applied to [012] (Ref. 4) and [110] (Ref. 1) superlattices. Similar calculations were recently published by Ren *et al.*¹⁹ using a rigid-ion model. In our calculations we simulated the superlattice by merely changing the cation masses (from Ga to Al masses), using for both constituents the force constants which gave the best fit to the bulk GaAs dispersion curves.¹⁵ *Ab initio* calculations of Baroni *et al.*²⁰ of the AlAs dispersion support the mass-change model except for an upward shift of the LO-mode frequencies.

As mentioned above, the [111] superlattice has C_{3v} point-group symmetry. The Brillouin zone of the [111] superlattice with an odd number of layers per unit cell (with a smaller number of layers for clarity) is depicted in Fig. 6. The longitudinal zone-center modes polarized parallel to the layer axis transform according to the one-dimensional irreducible representation A_1 and the perpendicularly polarized transverse modes according to the two-dimensional representation E . This classification remains valid for nonvanishing wave vectors along the [111] direction. Figure 7 shows calculated dispersion curves for the [111] $(\text{GaAs})_9/(\text{AlAs})_{10}$ structure. The regions $Y-\Gamma$, $\Gamma-Z$, and $W-\Gamma$ give the spatial dispersion along the three principal superlattice axes. The two $\Gamma-\Gamma$ portions show the directional dispersion for infinitesimally small wave vectors. The dispersion curves along the zone boundary can be found in the $Z-W-X$ portion.

An energy gap exists over the hole Brillouin zone between the AlAs-like optical region (320 to 400 cm^{-1}) and the corresponding GaAs-like region (from about 220 to 294 cm^{-1}). The GaAs-like optical-mode frequencies are separated from the bulk acoustical frequency region by local gaps related to anticrossings.

A. Folded and confined modes

The $\Gamma-Z$ portion ($q \parallel [111]$) shows the series of folded TA (degenerate) and LA phonons. The former exhibit lo-

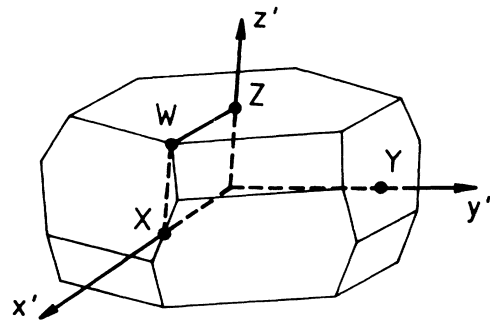


FIG. 6. Brillouin zone of the [111] superlattice (trigonal structure, C_{3v} symmetry). There is no standard notation for those points on the Brillouin-zone boundary which are denoted here by W , X , and Y .

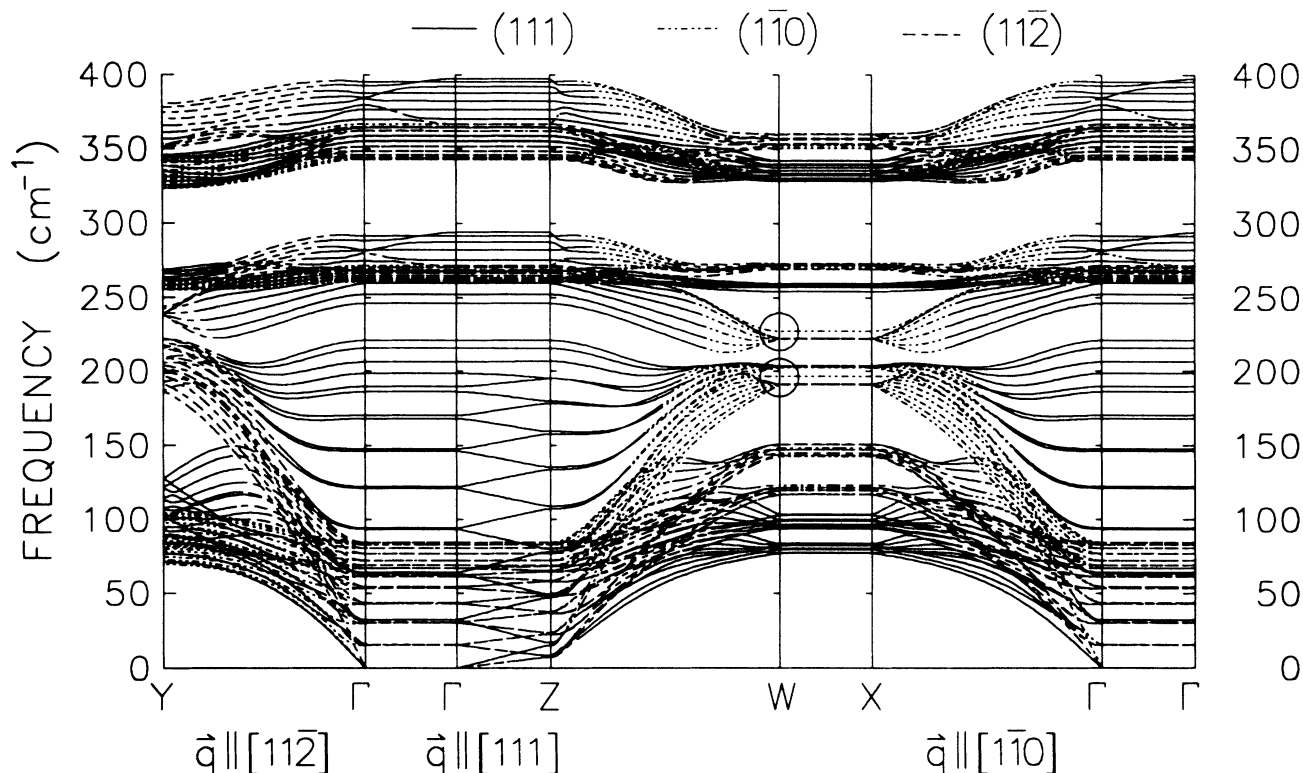


FIG. 7. Spatial and directional phonon dispersion curves for a $[111]$ $(\text{GaAs})_9/(\text{AlAs})_{10}$ superlattice. For the notation of the high-symmetry points of the Brillouin zone see Fig. 6. The two $\Gamma - \Gamma$ portions show the directional dispersion obtained by rotating a very small wave vector from parallel to $[111]$, the growth direction, to the perpendicular directions $[11\bar{2}]$ and $[1\bar{1}0]$. The different types of lines refer to the different dominating displacement polarizations.

calization (to the AlAs layers) even at low frequencies, between 70 and 90 cm^{-1} , and the latter between 200 and 220 cm^{-1} . This is due to lack of overlap of the bulk GaAs and AlAs acoustic bands in these frequency regions. The optical modes are all confined. This is quali-

tatively similar to the behavior in all the other investigated GaAs/AlAs structures.^{1,3-5,16}

Figures 8(a) and 8(b) gives the displacement pattern for the first two GaAs-like LO_m and TO_m modes. Shown are the magnitudes of the weighted displacement vectors

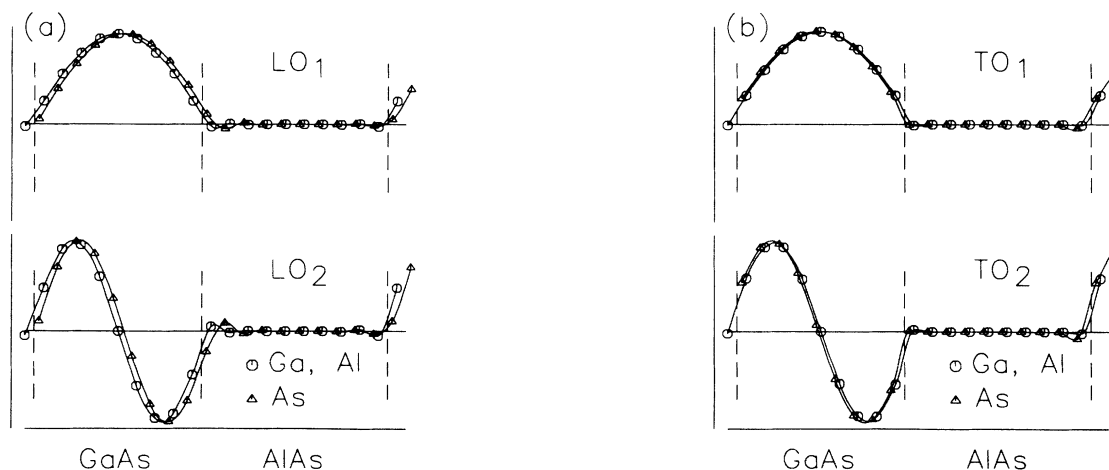


FIG. 8. Displacement pattern \mathbf{v} , Eq. (6), of (a) LO_m and (b) TO_m confined GaAs-like zone-center modes of the $[111]$ $(\text{GaAs})_9/(\text{AlAs})_{10}$ superlattice. The frequencies of the confined modes are 393.93 cm^{-1} (LO_1), 391.76 cm^{-1} (LO_2), 271.72 cm^{-1} (TO_1), and 270.57 cm^{-1} (TO_2). The layer boundaries (dashed lines) are taken to be the bisector planes of boundary Ga and As layers. The symbols mark the value of the nonzero component of \mathbf{q} at the positions along the superlattice axis of the Ga and Al (circles) and As (triangles) atomic planes. The lines through the symbols (for anion and cation displacements separately) are guides to the eye.

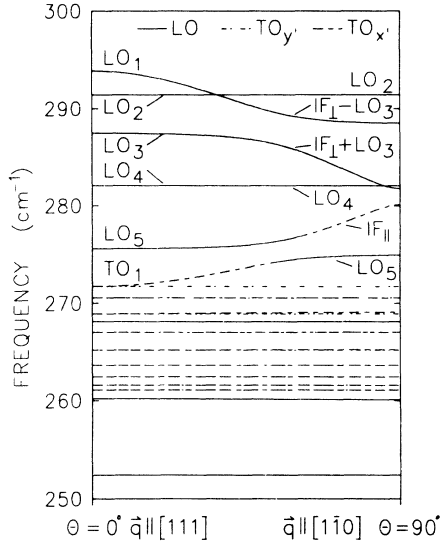


FIG. 9. Calculated angular dispersion of the optical modes of a $[111]$ $(\text{GaAs})_9/(\text{AlAs})_{10}$ superlattice for an infinitesimally small q with \mathbf{q} in the $(11\bar{2})$ plane. The solid lines refer to the LO modes polarized along z' , while the dashed and the dash-dotted lines correspond to TO_x and TO_y polarizations. Identical dispersion curves (but different polarizations) are obtained for \mathbf{q} in the $(1\bar{1}0)$ plane.

\mathbf{v}_k defined by

$$\mathbf{v}_k = \pm \mathbf{M}_k \mathbf{u}_k \quad (6)$$

for $\mathbf{q}=\mathbf{0}$, cf. Eq. (5). The positive sign applies to cations, the negative one to anions. As can be seen in Fig. 8, the cation-weighted displacements can be described by a sinusoidal dependence on layer position. The envelope function of the anion displacements is shifted against that of the cation displacements. Note that there is no symmetry element in C_{3v} , which would allow a classification of the modes in terms of even and odd parity. However, there is an additional symmetry built into the model by use of the same coupling of the As ions to the Ga as to the Al ions, which leads to inversion symmetry within the (Ga,Al) sublattice (see the Appendix) and, in fact, to even and odd Ga- and Al-sublattice displacement patterns for the modes with $\mathbf{q}||[111]$. This argument does not hold for the As sublattice. In principle, the center of mass of the whole superlattice unit cell is fixed. It seems, however, that neighboring layers tend to keep a nearly fixed center of mass, and this, together with the even-odd classification of the (Ga,Al)-sublattice displacements, forces an approximate even-odd classification also on the As-sublattice displacements. In reality, there is a small deviation from the force-constant symmetry of our model, but this is expected to lead to only weak violation of the even-odd symmetry. This fact then explains the absence of TO_m (m even) modes in Fig. 3 (except for a weak TO_2).

In our calculations, the confined modes with $\mathbf{q}||[111]$ have eigenvectors whose sinusoidal dependence can be described by the effective wave vectors q_m of Eq. (3). For confined LO_m and TO_m modes we find best agreement

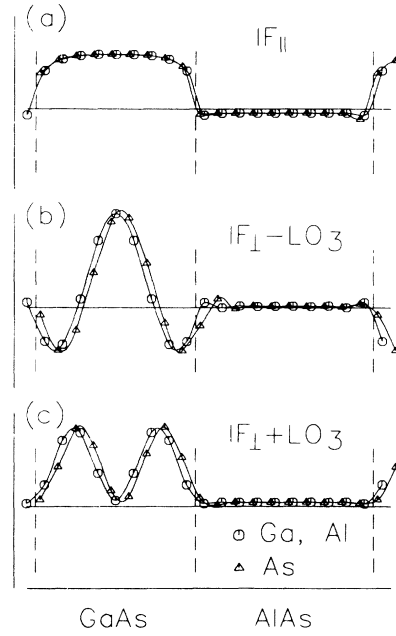


FIG. 10. Displacement pattern of GaAs-like electrostatic interface modes with $q \approx 0$ and $q \perp [111]$. Part (a) shows the displacement of the interface mode with polarization parallel to \mathbf{q} (in the layer planes, with frequency 280.14 cm^{-1}). Parts (b) and (c) refer to a pair of modes with polarization along z' (perpendicular to the layer planes, with frequencies 288.50 and 281.78 cm^{-1}).

with the bulk modes for $\gamma \approx 0.5$. With this choice of γ the frequencies of these modes map closely to the $\omega(\mathbf{k})$ bulk dispersion branches; see Figs. 4(a) and 4(b). This result is supported by the GaAs displacement vector components, given in Figs. 8(a) and 8(b), penetrating into the AlAs layers in a way corresponding to $\gamma \approx 0.5$.

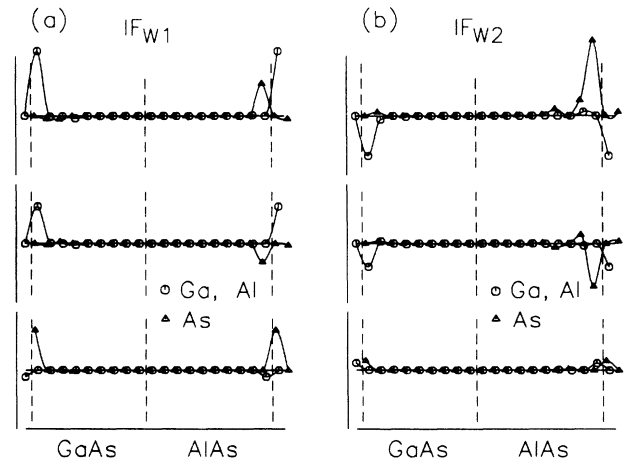


FIG. 11. Displacement pattern of the interface modes IF_{W1} and IF_{W2} with wave vector at the W point on the Brillouin-zone boundary with frequencies of (a) 227.45 cm^{-1} and (b) 196.62 cm^{-1} . Shown are the components of the displacement vectors \mathbf{v} , Eq. (6), along $[1\bar{1}0]$, $[11\bar{2}]$, and $[111]$ (from top to bottom).

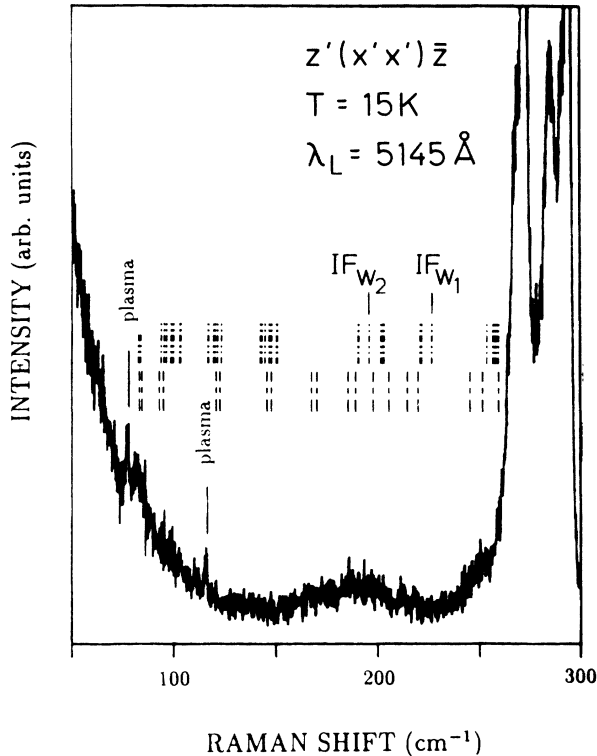


FIG. 12. Raman spectra of a [111] $(\text{GaAs})_9/(\text{AlAs})_{10}$ superlattice at 15 K in the $z'(x'x')\bar{z}$ backscattering configuration. Indicated are the frequencies of the zone-boundary ($X-W$) modes, including, in particular, the interface modes IF_{W_1} and IF_{W_2} (cf. Fig. 11) (upper series) and those of the folded-zone-center modes (lower series). The exciting-laser line is at $\lambda_L = 51.45 \text{ \AA}$.

B. Directional dispersion and interface modes

Rotating a very small wave vector away from the superlattice axis the frequencies of the corresponding LO_m modes, which have a dipole moment along this axis, decrease while those of the TO_m modes with perpendicular polarization increase. At the same time these modes take up the character of electrostatic interface modes.²¹ This directional dispersion is shown in the $\Gamma-\Gamma$ portions of Fig. 7 and, enlarged, in Fig. 9. By symmetry, the angular dispersion in the $(1\bar{1}0)$ wave-vector plane should be the same as that in the $(11\bar{2})$ plane. Due to the lack of inversion or reflection plane all confined LO_m and TO_m modes should display some directional dispersion and anticrossings (at least for small values of m), but, as can be seen in Fig. 9, this is not so for even values of m . In this case, as mentioned above, the anion displacements can be rather well approximated by even functions. These modes have vanishing dipole moment and do not couple to the macroscopic field.

Figure 10 shows the displacement pattern for the electrostatic interface modes. The IF_{\parallel} mode, polarized parallel to the layer plane, shows the typical displacement pattern of interface modes, with exponentially decaying penetration into the AlAs layer and a nearly constant displacement in the GaAs layer. The modes polarized per-

pendicular to the layers, $\text{IF}_{\perp}\pm\text{LO}_3$, are in the GaAs region superpositions of an IF-like constant displacement with a LO_3 -like sinusoidal component.

In directions perpendicular to the layer axis ($\Gamma-X, \Gamma-Y$) the phonon branches show strong dispersion ending in narrow bands at the zone-boundary. In the $W-X$ portion of Fig. 7, which corresponds to a zone edge parallel to the layer axis, all modes are localized. Some phonon branches are well separated at the clusters of narrow bands. For two of these modes the displacement patterns are shown in Fig. 11. Both modes have frequencies in the overlapping region of the optic GaAs and acoustic AlAs energy bands. They are highly localized at the interfaces. Interface imperfections would make these modes Raman active, and possible experimental evidence of these highly localized zone-boundary interface modes is given in Fig. 12. Another interpretation of the structures shown in Fig. 12 is based on the defect-induced activity of the other zone-boundary modes with the same frequency and a large density of states or the activity of the backfolded acoustic AlAs phonons.

VI. SUMMARY

We have investigated the phonon properties of a $(\text{GaAs})_9/(\text{AlAs})_{10}$ superlattice grown along the [111] direction by MBE on a $(111)B$ GaAs substrate tilted by 0.5° . The appearance of distinct x-ray satellite peaks demonstrates the formation of highly ordered periodic superlattice structures. We have observed confined LO and TO modes with frequencies close to those of the optical phonons of the parent materials in the $\Gamma-L$ direction ($\mathbf{q} \parallel [111]$) of \mathbf{k} space. Also, folded-acoustic-phonon doublets of longitudinal polarization, whose frequencies are in agreement with shell-model calculations, have been seen.

Using a shell model we have calculated the phonon frequencies, phonon dispersion curves, and eigenvectors of a [111] $(\text{GaAs})_9/(\text{AlAs})_{10}$ superlattice. The calculated normal-to and in-plane modes show good agreement with measured TO and LO confined- and interface-mode frequencies in the GaAs optical-phonon region. The symmetry properties of these superlattices and their vibrations have been investigated. A curious paritylike behavior of the confined modes, related to the additional symmetry introduced by the use of the same force constants for AlAs as for GaAs, has been found.

ACKNOWLEDGMENTS

The technical assistance of A. Fischer with the MBE growth and H. Hirt, M. Siemers, and P. Wurster with Raman measurements is gratefully acknowledged. Thanks are also due to W. Kress for enlightening discussions of the symmetry properties. Part of this work was sponsored by the Bundesministerium für Forschung und Technologie of the Federal Republic of Germany. Z.V.P. gratefully acknowledges financial support from the Alexander von Humboldt Foundation (Bonn, Federal Republic of Germany).

APPENDIX

In this Appendix we want to state the assumptions and arguments leading to the even-odd classifications of the (Ga,Al) displacements of the vibrations with wave vector in the growth direction, q_{\parallel} [111]. For these modes one has to consider only the vibrations of planes (of like atoms) against each other, and the problem is reduced to that of a one-dimensional chain.

One has to distinguish between the planes of Ga and Al atoms on the one hand and of the As atoms on the other, which is done by labeling the Ga and Al planes by m, m' (including 0), and the As planes by n, n' , etc. The distance of planes with neighboring m and m' (or n and n') is equal to the thickness of a pair of monolayers, $d_1 = d_2 = a_0/\sqrt{3}$, cf. Sec. II. The force constant between planes with indices k and k' ($k = m$ or $k = n$) is denoted by $\Phi(k, k')$.

In addition to the assumption $d_1 = d_2$ (which is not essential for our reasoning), one assumes that AlAs differs from GaAs only in the cation mass. This means that the coupling between the atoms is independent of whether these belong to the GaAs or AlAs or interface region and that the force constants

$$\Phi(k, k') = \Phi(k + m', k' + m')$$

are invariant against translation by multiples (m') of d_i .

We partition the matrix of force constants into two submatrices with elements referring to the Ga and Al atoms (index 1) and to As atoms (index 2),

$$\Phi = \begin{pmatrix} \Phi_{11} & \Phi_{12} \\ \Phi_{21} & \Phi_{22} \end{pmatrix},$$

and analogously for the masses.

One will need the matrix

$$G_{22} = (\Phi_{22} - \omega^2 M_{22})^{-1}.$$

The translational invariance of the As-As interaction, Φ_{22} , and of their masses, M_{22} , is also reflected in G_{22} ,

$$G_{22}(n, n') = G_{22}(n + m', n' + m').$$

The effective interaction between the planes of the (Ga,Al) atoms is the sum of the direct interactions,

$\Phi_{11}(m, m')$, and of the interaction mediated by the As planes,

$$\Phi'(m, m') = - \sum_{n, n'} \Phi_{12}(m, n) G_{22}(n, n') \Phi_{21}(n', m').$$

This is obtained by formally eliminating the As degrees of freedom from the equations of motion.

It is obvious that the direct interaction Φ_{11} has inversion symmetry,

$$\Phi_{11}(0, m) = \Phi_{11}(0, -m).$$

That this is also true of the indirect interaction $\Phi'(0, m)$ is seen as follows. One uses the translational invariance of the interactions (and of G_{22}) to write

$$\begin{aligned} \Phi'(0, -m) &= - \sum_{n, n'} \Phi_{12}(0, n) G_{22}(n, n') \Phi_{21}(n', -m) \\ &= - \sum_{n, n'} \Phi_{12}(m, n + m) G_{22}(n + m, n' + m) \\ &\quad \times \Phi_{21}(n' + m, 0). \end{aligned}$$

Change of the dummy indices n and n' leads to

$$\Phi'(0, -m) = - \sum_{n, n'} \Phi_{12}(m, n) G_{22}(n, n') \Phi_{21}(n', 0).$$

Newton's third law implies

$$\Phi_{12}(m, n) = \Phi_{21}(n, m),$$

$$\Phi_{22}(n, n') = \Phi_{22}(n', n),$$

and thus also

$$G_{22}(n, n') = G_{22}(n', n),$$

a fact which leads to

$$\begin{aligned} \Phi'(0, -m) &= - \sum_{n, n'} \Phi_{21}(n, m) G_{22}(n', n) \Phi_{12}(0, n') \\ &= \Phi'(0, m), \end{aligned}$$

i.e., inversion symmetry.

Note that the analogous arguments cannot be made for the indirect interaction of the As planes since the Ga and Al masses (in the resolvent G_{11}) do not have translational symmetry.

*Permanent address: Institute of Physics, P.O. Box 57, YU-11000 Belgrade, Yugoslavia.

¹Z. V. Popović, M. Cardona, E. Richter, D. Strauch, L. Tapfer, and K. Ploog, *Phys. Rev. B* **40**, 3040 (1989).

²D. Kirillov and Y. C. Pao, in *Materials Research Society Symposium Proceedings*, edited by R. T. Tung, L. R. Dawson, and R. L. Gunshor (MRS, Pittsburgh, 1988), Vol. 102, p. 169.

³Z. V. Popović, M. Cardona, L. Tapfer, K. Ploog, E. Richter, and D. Strauch, *Appl. Phys. Lett.* **54**, 846 (1989).

⁴Z. V. Popović, M. Cardona, E. Richter, D. Strauch, L. Tapfer, and K. Ploog, *Phys. Rev. B* **40**, 1207 (1989).

⁵Z. V. Popović, H. J. Trodahl, M. Cardona, E. Richter, D. Strauch, and K. Ploog, *Phys. Rev. B* **40**, 1202 (1989).

⁶T. Hayakawa, K. Takahashi, M. Kondo, T. Suyama, S. Yamamoto, and T. Hijikata, *Phys. Rev. Lett.* **60**, 349 (1989).

⁷T. Hayakawa, M. Kondo, T. Suyama, K. Takahashi, S. Yamamoto, and T. Hijikata, *Jpn. J. Appl. Phys.* **26**, L302 (1987).

⁸Y. Kajikawa, N. Sugiyama, T. Kamijoh, and Y. Katayama, *Jpn. J. Appl. Phys.* **28**, L1022 (1989).

⁹L. W. Mohlenkamp, G. E. W. Bauer, R. Eppenga, and C. T. Foxon, *Phys. Rev. B* **38**, 6147 (1988).

¹⁰S. Subbanna, H. Kroemer, and J. L. Merz, *J. Appl. Phys.* **59**, 488 (1986).

¹¹B. Jusserand and M. Cardona, in *Light Scattering in Solids V*, edited by M. Cardona and G. Güntherodt (Springer-Verlag, Heidelberg, 1989), p. 49; J. L. Merz, A. S. Barker, Jr., and A. C. Gossard, *Appl. Phys. Lett.* **31**, 117 (1987); R. Merlin, C. Colvard, M. V. Klein, H. Markoc, A. Y. Cho, and A. C. Gossard, *ibid.* **36**, 43 (1980).

- ¹²J. Kervarec, M. Baudet, J. Caulet, P. Auvray, J. Y. Emery, and A. Regreny, *J. Appl. Crystallogr.* **17**, 196 (1984); see also L. Tapfer and K. Ploog, *Phys. Rev. B* **33**, 5565 (1986).
- ¹³A. K. Sood, J. Menéndez, M. Cardona, and K. Ploog, *Phys. Rev. Lett.* **54**, 2115 (1985).
- ¹⁴G. Dolling and J. L. T. Waugh, in *Lattice Dynamics*, edited by R. F. Wallis (Pergamon, Oxford, 1965), p. 19.
- ¹⁵D. Strauch and B. Dorner, *J. Phys. C* (to be published).
- ¹⁶E. Richter, D. Strauch, *Solid State Commun.* **64**, 867 (1987).
- ¹⁷C. Kittel, *Introduction to Solid State Physics*, 3rd ed. (Wiley, New York, 1953), p. 121.
- ¹⁸*Landolt-Börnstein*, Vol. 17a, *Physics of Group IV Elements and III-V Compounds*, edited by O. Madelung (Springer, Berlin, 1982), p. 235.
- ¹⁹S. F. Ren, H. Chu, Y. C. Chang, *Phys. Rev. B* **40**, 3060 (1989).
- ²⁰S. Baroni, P. Giannozzi, E. Molinari, in *Proceedings of the 6th International Conference on Phonon Scattering in Condensed Matter*, edited by S. Hunklinger and W. Ludwig (World Scientific, Singapore, in press).
- ²¹R. E. Camley and D. L. Mills, *Phys. Rev. B* **29**, 1685 (1984).